Active Light Control of the MoS_2 Monolayer Exciton Binding Energy

Ziwei Li,[†,∥] Yingdong Xiao,[†,∥] Yongji Gong,[‡] Zongpeng Wang,[†] Yimin Kang,[†] Shuai Zu,[†] Pulickel M. Ajayan,[‡] Peter Nordlander,[§] and Zheyu Fang*[,†]

[†]School of Physics, State Key Lab for Mesoscopic Physics, Academy for Advanced Interdisciplinary Studies, Peking University, Beijing 100871, China and [‡]Department of Materials Science and NanoEngineering and [§]Department of Electrical and Computer Engineering, and Laboratory for Nanophotonics, Rice University, 6100 Main Street, Houston, Texas 77005, United States. [∥]Z.L. and Y.X. contributed equally to this work.

ABSTRACT Plasmonic excitation of Au nanoparticles deposited on a MoS_2 monolayer changes the absorption and photoluminescence characteristics of the material. Hot electrons generated from the Au nanoparticles are transferred into the MoS_2 monolayers, resulting in n-doping. The doping effect of plasmonic hot electrons modulates the dielectric permittivity of materials, resulting in a red shift of both the absorption and the photoluminescence spectrum. This spectroscopic tuning was further investigated experimentally by using different Au nanoparticle concentrations, excitation laser wavelengths, and intensities. An analytical model for the photoinduced modulation of the MoS_2 dielectric function and its exciton binding energy change is developed and used to estimate the doping density of plasmonic hot electrons. Our approach is important for the development of photonic devices for active control of light by light.

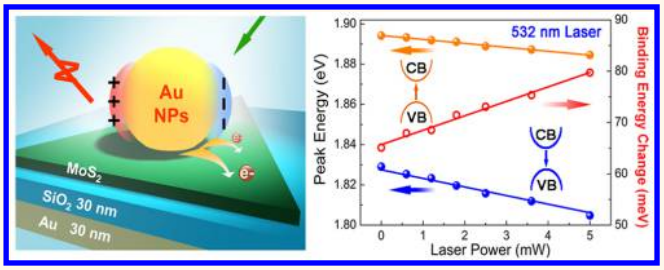

KEYWORDS: plasmonic hot electron · MoS_2 · absorption · exciton · active tuning

Molybdenum disulfide (MoS_2) monolayers are atomic thickness two-dimensional semiconductors with intriguing physical properties.[1,2] Because of their unique electronic and optical characteristics, it has been suggested that MoS_2 monolayers may play an important role in future optoelectronic devices. Tightly bound excitons[3] in the MoS_2 monolayers are efficiently formed by light absorption and result in a strong photoluminescence (PL) emission.[4,5] The absorption of a MoS_2 monolayer is determined by its band structure and carrier density.[6] Significant recent efforts have been devoted to extrinsically control the PL spectrum of MoS_2 monolayers, including gate-bias tuning,[7,8] physical adsorption,[9] and chemical doping.[10,11] While the optical cross sections of individual monolayers are very weak, photonic crystal microcavities can be used to enhance the absorption[12,13] and tune the PL emission.[14] However, to date, few studies have reported light control of absorption in MoS_2 monolayers.

Surface plasmons with their outstanding light-trapping and electromagnetic field enhancement properties can play an important role in a wide range of optoelectronics and nanophotonics applications, such as optical tweezers,[15,16] photovoltaics,[17,18] and subwavelength optical devices.[19,20] Plasmonic hot electrons generated from nonradiative plasmon decay have been explored in photodetection[21,22] and photocatalysis applications.[23] Plasmon-induced hot electron generation has also been used to dope and control the conductivity of graphene[24] as well as induce phase transitions in an adjacent MoS_2 monolayer at low temperatures and controlled environments.[25] Two-dimensional (2D) materials are particularly sensitive to charge injection due to their confinement, and plasmonic hot carrier generation provides a unique opportunity for active control of their properties.

In this study, we use plasmon-induced hot carrier generation to dope and control both the optical absorption and photoluminescence of a MoS_2 monolayer. Au nanoparticles were deposited at various concentrations on the MoS_2 and illuminated by laser light at different wavelengths and intensities. The absorption spectra of the structure were measured independently using a separate light source and found to

* Address correspondence to zhyfang@pku.edu.cn.

Received for review June 21, 2015 and accepted September 8, 2015.

Published online September 08, 2015
10.1021/acsnano.5b03764

exhibit both intensity changes and red shifts that depend on the nanoparticle excitation conditions. The largest spectral shifts were observed at laser wavelengths corresponding to nanoparticle plasmon excitation. These red shifts were found to increase monotonically with laser intensity and nanoparticle concentration. We also measured the PL shifts as a function of nanoparticle excitation conditions and found a significant red shift of the PL. Both results can be explained by the modulation of the dielectric permittivity with the exciton binding energy.

RESULTS AND DISCUSSION

The chemical vapor deposition (CVD)-grown MoS_2 monolayers were first transferred onto a substrate using the poly(methyl methacrylate) (PMMA) nanotransfer method and then covered by 5 nm diameter Au nanoparticles (Au NPs) at different concentrations. As illustrated in Figure 1a, the substrate consists of 30 nm SiO_2 film on a 30 nm thick Au mirror fabricated using E-beam evaporation. With white light illumination, reflectance spectra of the MoS_2 monolayer were measured and modulated by the separate excitation laser. The schematic of the experimental setup is shown in Supporting Information S1. Figure 1b is an optical image of the MoS_2 structure covered with 5 mg L^{-1} Au NPs. The edge length of the MoS_2 triangle is ~100 μm. Figure 1c shows the absorption of the MoS_2–Au hybrid film on the SiO_2/Si substrate and MoS_2 film on SiO_2/Au and SiO_2/Si, which are obtained from the reflectance spectra under white light illumination (the absorption of ultrathin films is directly proportional to the differential of reflectivity). The two main peaks at 660 nm (peak A) and 615 nm (peak B) are direct band gap transitions, which are characteristic absorption features of MoS_2 monolayers. The energy difference of peak A and peak B results from the spin–orbital coupling in the split valence band. The 8% increase in absorption when the 30 nm Au mirror was present is due to multiple reflection and absorption enhancement.[12] The measured absorption change due to the mirror is in excellent agreement with the simulation results in Figure 1d (see additional details in the Materials and Methods section). A 532 nm laser was used to excite the surface plasmon resonance (SPR) of the Au NPs. Both the PL spectra and Raman spectra for the MoS_2 monolayer with and without Au NPs are shown as Figure S2 in Supporting Information, which shows the presence of plasmonic hot electron doping effects.[25,26]

Au NPs with various concentrations ranging from 5 to 15 mg L^{-1} were pipetted and spin-coated onto the MoS_2 monolayers. Figure 2a shows the variations of absorption without 532 nm excitation. With increasing NP concentration, the absorption intensity decreases because the reflection and scattering efficiencies of the Au NP layer increases with NP concentration. However, when the laser is turned on (Figure 2b), clear red shifts of both absorption features A and B are apparent. In Figure 2c,d, the peak wavelength and intensity

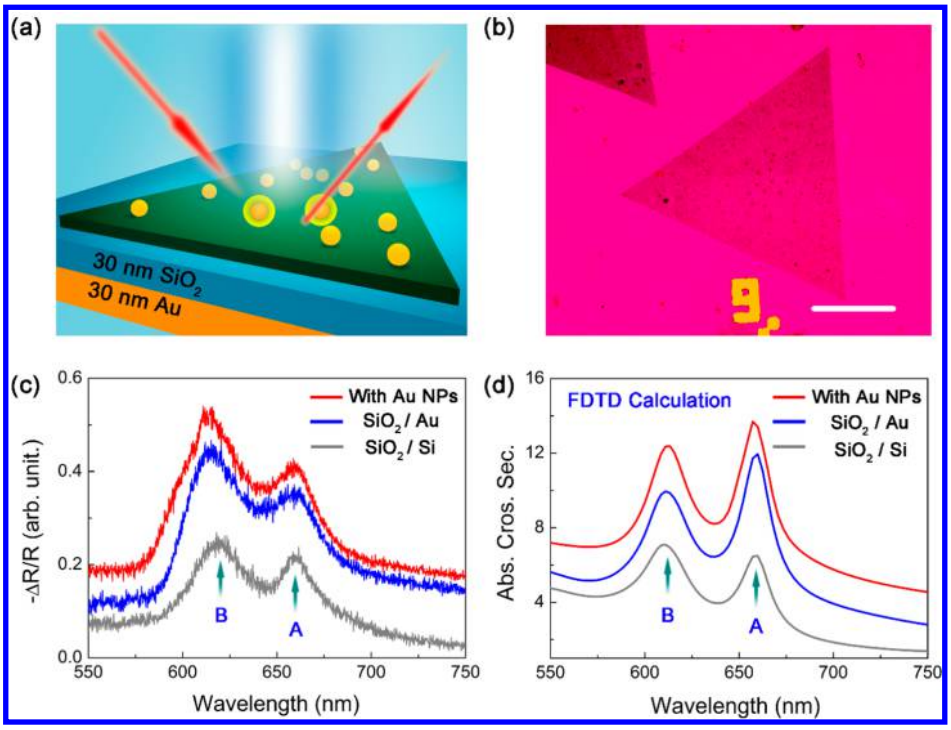

Figure 1. (a) Schematic of MoS_2–Au hybrid film under 532 nm laser excitation and white light illumination. The substrate consists of 30 nm SiO_2 film on a 30 nm thick Au mirror. (b) Optical image of the MoS_2 monolayer under a 100× objective lens (scale bar is 30 μm). (c) Absorption spectra of the MoS_2–Au hybrid film on a SiO_2/Si substrate (red) and MoS_2 film on SiO_2/Au (blue) and on SiO_2/Si (gray). The concentration of the Au NPs is 10 mg L^{-1}. (d) Absorption cross section simulated by FDTD.

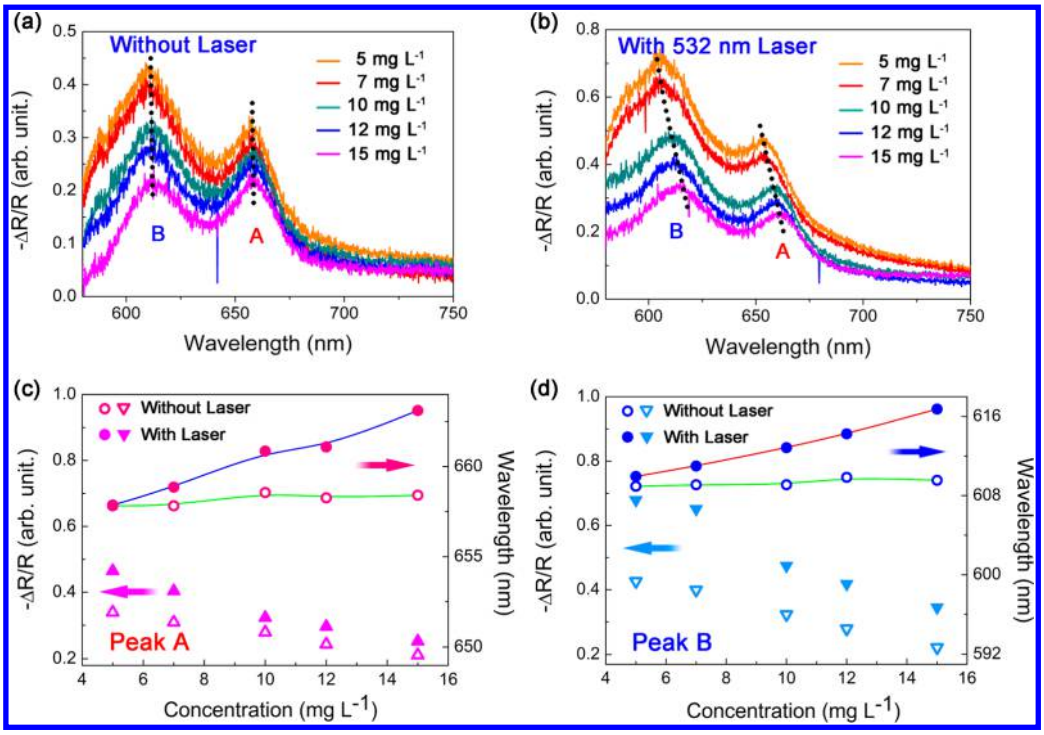

Figure 2. Absorption spectra without (a) and with (b) 532 nm laser illumination as a function of Au NP concentrations ranging from 5 to 15 mg L^{-1}. Peak wavelength (circles) and intensity variations (triangles) of peak A (c) and peak B (d) with (solid symbols) and without (hollow symbols) laser excitation. The laser power is 1 mW.

variations of A and B are plotted as a function of Au NP concentration. When illuminated, peak A red shifts from 658 to 663 nm when the Au concentration increased from 5 to 15 mg L^{-1}. Peak B experiences a red shift smaller than that of peak A but exhibits a larger intensity attenuation. Both the red-shifting and intensity attenuation are consistent with an n-doping effect reported in previous work.[6]

Figure 3 shows how the optical properties depend on laser power for 15 mg L^{-1} NP concentration. Figure 3a shows a PL red shift from 678 to 690 nm as the laser power increases from 0.01 to 5 mW, which is also consistent with plasmon-induced doping.[25,27] The effect from laser-induced doping[28] of MoS_2 monolayers (without Au NPs) is also compared and analyzed in the Supporting Information (Figure S6). The absorption spectra in Figure 3b shows a similar laser intensity dependence as the PL with a 15 nm red shift when the laser power increased to 5 mW. The intensity decrease with increasing laser power is further evidence for plasmonic hot electron doping of the conduction band. Because of the Pauli exclusion principle, an increase of the carrier density reduces the density of available final states.[6]

The efficient generation of plasmonic hot electrons requires excitation of the surface plasmon resonance of the Au NPs. To further confirm the hot electron doping effect, the dependence of MoS_2 absorption spectra on the incident laser wavelength was investigated and is shown in Figure 4. The laser power was kept at 2.5 mW for all wavelengths. Figure 4a shows that only for resonant excitation of the dipolar plasmon at 532 nm do the two absorption features A and B exhibit significant shifts. For 442 nm near the dipolar plasmon resonance, we observed a small red shift. The absorption for 325 nm (blue line) and 633 nm (purple line) excitations is very similar to what is observed without excitation (black line). The calculated absorption cross section of the 5 nm sized Au NPs is shown in Figure 4b, where the peak (510 nm) represents the significant efficient absorption due to dipolar resonance. Only for resonant excitations of Au NP plasmons do we expect significant hot carrier generation and significant doping. Figure 4c shows that the absorption features of the MoS_2−Au hybrid structure are independent of incident laser polarization. This isotropic response is expected for spherical NPs.

Figure 5 illustrates the mechanism of the plasmonic hot electron tuning of MoS_2 monolayer optical properties. The excitation of the Au surface plasmon at 532 nm generates hot electrons that can transfer into the MoS_2 conduction band and induce a n-doping. Because the work function of Au is around 5.1 eV, with an excitation laser of 532 nm, the plasmonic hot electron distribution will extend up to 2.8 eV above the Fermi level and can readily transfer across the Schottky barrier (<0.8 eV) at the Au/MoS_2 interface.[25] The doping carriers contribute a Drude term to the permittivity of the MoS_2 monolayer and thus increase the binding energy of the exciton, which results in a red

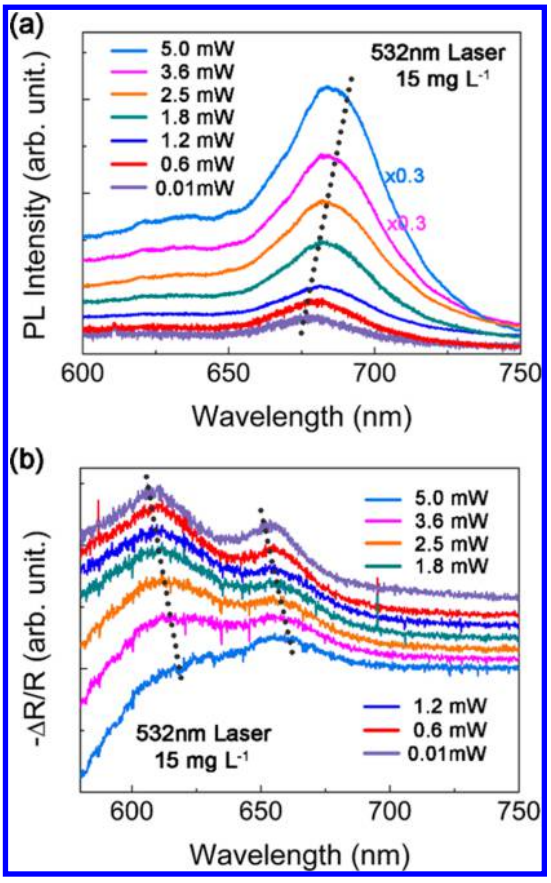

Figure 3. (a) PL spectra and (b) absorption spectra of the MoS_2 structure with 15 mg L^{-1} NP concentration for laser powers ranging from 0.01 to 5 mW. The excitation laser wavelength is 532 nm.

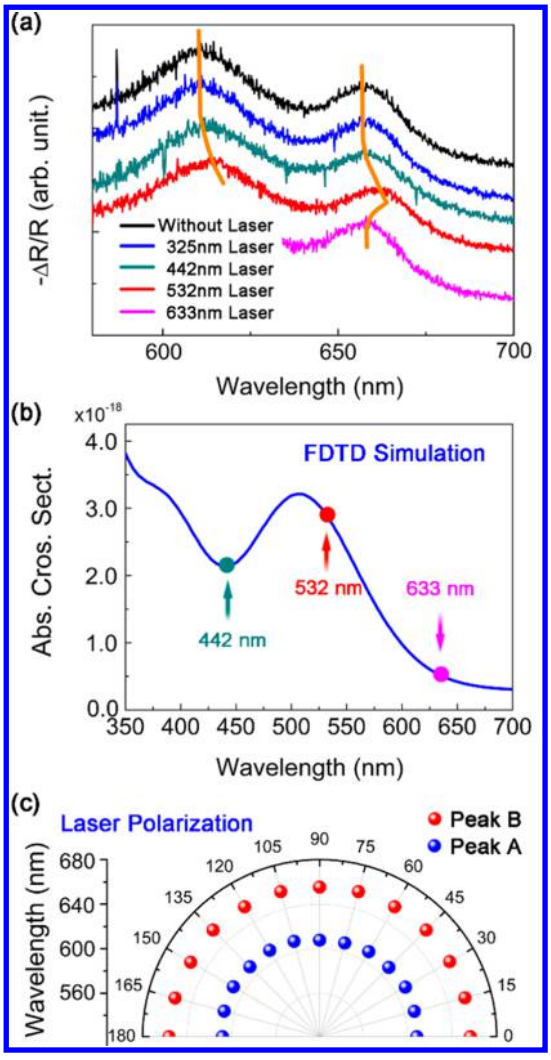

Figure 4. (a) Dependence of the MoS_2 monolayer absorption peaks on the incident laser wavelength for a NP density of 15 mg L^{-1}. (c) Absorption cross section of a 5 nm Au NP simulated by FDTD. Three color symbols correspond to different incident lasers. (c) Absorption spectra of peak A and peak B as a function of laser incident polarizations.

shift of the absorption spectrum. As the exciton binding energy is increased, the absorption peak red shifts. The band structure of MoS_2 monolayers is plotted at the right side of Figure 5. The yellow arrow represents the absorption process of peak A and the electronic transition from the top of the valence band to a final state above the excitonic level. After the absorption, the excited electrons nonradiatively relax into the excitonic level (white dashed line) and subsequently generate the luminescence (blue arrow). With increased nanoparticle concentration or incident laser power, the doping level and corresponding binding energy of the exciton increases, which induces a red shift of both the absorption and the luminescence.

In Figure 6, we plot the energy of the luminescence peak and the absorption feature A as a function of laser power (data from Figure 3). The exciton binding energy can be obtained by using $E_b = E_g - E_{PL}$,[29,30] where the E_g is the band gap of the MoS_2 monolayer. Because of the doping and its influence on the exciton energy, the measured absorption peak energy is not exactly the same as the band gap and cannot directly be used to calculate the value of the exciton binding energy. In this work, we use the difference between the absorption and PL peaks as a probe of the exciton binding energy and to investigate its dependence on doping. Thus, as the incident laser power changed from 0.01 to 5 mW, the ΔE_b = 15 meV shift obtained from the red line of Figure 6 is the change of the exciton binding energy induced by hot electron doping.

To qualitatively explain the blue shift of the exciton binding energy with doping density, we model the MoS_2 exciton as a 2D hydrogen atom by neglecting confinement effects. The energy levels of the 2D hydrogen-like atom are[31]

$$E_b = \frac{\mu e^4}{2\epsilon_0^2 \epsilon_r^2 \hbar^2 \left(n - \frac{1}{2}\right)^2} \quad (1)$$

where μ is the reduced effective mass of the electron–hole pair, n is the quantum number (as assumed n = 1), and ϵ_r is the relative permittivity of the MoS_2 structure, which is as assumed to be equal to the static

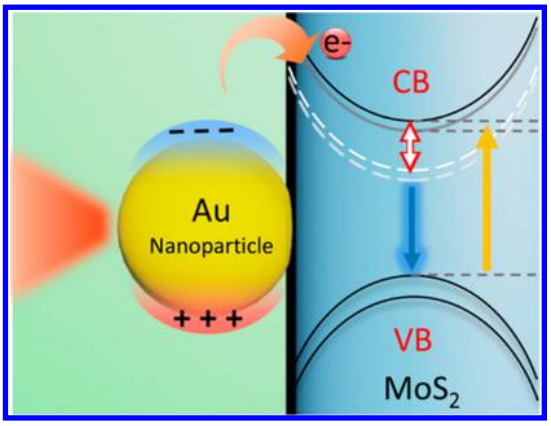

Figure 5. Schematic view of the interaction between Au nanoparticles and MoS_2 monolayers. The white dashed line represents excitonic energy level. The yellow arrow represents the absorption process of the peak A, an electronic transition from the upper spin−orbit split valence band to the conduction band (peak B is due to excitation from the lower spin−orbit split valence band but not shown). The blue arrow represents the PL emission. The hollow arrow represents the tunable binding energy change of the exciton that is controlled by the doping level of the conduction band.

value of 4.26.[32] The change of exciton binding energy ΔE_b can be directly related to the relative permittivity $\Delta\epsilon_r$ as

$$\frac{\Delta\epsilon_r}{\epsilon_r} = \left(1+\frac{\Delta E_b}{E_b}\right)^{-1/2} - 1 \qquad (2)$$

For the exciton binding, the energy change is 15 meV and the E_b is ~0.5 eV;[33,34] $\Delta\epsilon_r/\epsilon_r$ is calculated as −0.015. As a consequence of the plasmonic hot electron doping, the Drude screening mechanism begins to contribute to the permittivity of the MoS_2. In the weak doping limit, the Drude term can simply be added to the intrinsic permittivity of MoS_2 and results in an effective permittivity:

$$\epsilon_r(\omega) = \epsilon_{opt} - \frac{Ne^2}{m^*\epsilon_0(\omega^2 + i\gamma\omega)} \qquad (3)$$

where m^* is the effective mass of the carriers, N is the electron number density, ω is the frequency, and γ is the Drude damping rate (which is assumed to be $\gamma \ll \omega$). The relevant frequency difference is the exciton binding energy change $\hbar\omega_2 - \hbar\omega_1 = \Delta E_b$. The carrier density then can be obtained from

$$\frac{N_2}{\omega_2^2} - \frac{N_1}{\omega_1^2} = \frac{-\Delta\epsilon_r m^*\epsilon_0 d}{e^2} \qquad (4)$$

where m^* ($0.44m_e$) is used in above equations,[32] and m_e is the mass of a free electron; d (0.67 nm) is the effective thickness of a MoS_2 monolayer. From eq 4, we then estimate the doping density due to injected plasmonic hot electrons as 2.6×10^{11} cm^{-2}. In this calculation, we

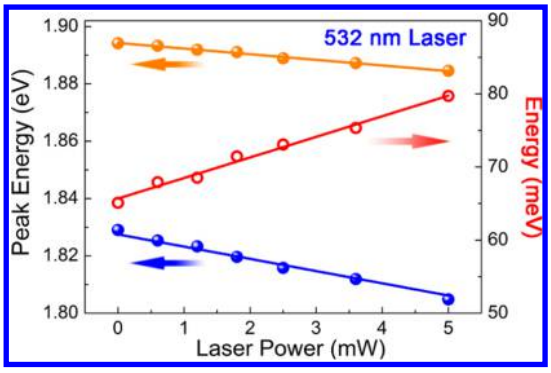

Figure 6. Absorption peak A (orange) and luminescence peak (blue) from Figure 3 as a function of laser power. The red line is the energy difference between the absorption and PL peak energy for each of the incident laser powers that changed from 0.01 to 5 mW.

can neglect the change in the Fermi level due to doping since it is much smaller than the observed exciton binding energy shift (15 meV) (see details in Supporting Information S7).

When the Au NP plasmons are excited, the resulting hot electron doping thus induces a modulation of the dielectric permittivity. This doping increases the exciton binding energy, resulting in a red shift of both the absorption and the photoluminescence spectra. In the experiment, the PL emission is, in principle, composed of contributions from both excitons and trions; however, at the present doping level (10^{11} cm^{-2}), which is much lower than that for chemical doping (~10^{13} cm^{-2}), the PL spectrum is dominated by the exciton, and the trion emission is negligible.

CONCLUSIONS

In summary, we have shown that plasmon excitation of Au nanoparticles on MoS_2 monolayers can enable active light control of MoS_2 exciton binding energy. The mechanism is plasmon-induced hot electron injection and doping of the monolayer. For resonant excitation of the nanoparticle plasmons, both the absorption and the photoluminescence spectra of the MoS_2 monolayer red shift. The magnitude of this optical tuning depends on Au nanoparticle concentration and incident laser wavelength. The exciton binding energy depends on the doping density. A model based on the Drude screening mechanism was developed and used to estimate the doping density as 2.6×10^{11} cm^{-2}. This work opens up a new strategy for the engineering a plasmon-based optoelectronic device for active control of light by light, such as highly sensitive photodetectors and plasmonic field-effect transistors.

MATERIALS AND METHODS

Preparation of MoS_2 Monolayers. MoS_2 samples were synthesized in a typical procedure by chemical vapor deposition method.[35] The sulfur (S) and molybdenum oxide (MoO_3) powder were utilized as the S and Mo sources, respectively. S powder was located at the upstream region of the furnace. MoO_3 powder placed in a boat was put into a fused quartz tube located at the center of the CVD furnace. A clean 275 nm SiO_2/Si

substrate was placed above the MoO_3 powder. With precise control of growing temperature, gas flow rate, and growing time, large-area MoS_2 monolayers with high quality were synthesized.

Preparation of MoS_2–Au Hybrid Structures. With an experiential wetting transfer process, MoS_2 monolayers can be transferred onto a 1D PC substrate. The CVD-grown MoS_2 monolayers were first spin-coated with PMMA and then baked on a hot plate with 180 °C for 5 min. SiO_2 layers were corroded when immersed in KOH solutions for 4 h at a concentration of 2 mol L^{-1}. Then, the PMMA films held MoS_2 monolayers floating on the liquid surface. A prepared substrate was used to fish out the PMMA films, which was rinsed several times with DI water. Finally, PMMA was removed with hot steam of acetone. The 5 nm tannic Au nanoparticle solutions (nano Composix) were pipetted and spin-coated on transferred MoS_2 monolayers.

Optical Measurement. All the spectra, including reflection, Raman, and PL, were measured by a home-built optical system. An iHR550 Raman spectrometer from Horiba was utilized with 600 and 2400 g mm^{-1} gratings. The Raman signals were detected using 2400 g mm^{-1} gratings for high resolution. The reflection and PL spectra were measured with 600 g mm^{-1}. The objective lens was at 50× magnification. Each spectrum was acquired in 8 s, with the purpose of minimizing the noise-to-signal ratio. The white light source was a Dolan-Jenner MI-150 with fiber illumination. The laser excitation was changed among 325, 442, 532, and 633 nm, where the beam was focused to a diffraction-limited spot (diameter $\sim 1\ \mu$m).

Absorption Cross Section of MoS_2. The absorption cross sections of MoS_2 monolayers were simulated by FDTD solutions. In the simulation, the Au NPs were distributed randomly on the surface of MoS_2 monolayers with corresponding concentrations. The absorption of MoS_2 was evaluated by integrating the pointing vector over the whole volume of MoS_2 layers. The refraction index of MoS_2 monolayers was extracted by parametrizing experimental data into a band and exciton transition (Brunaur–Emmett–Teller) model as reported in the previous work.[12] The imaginary part of the dielectric function can be written as

$$\epsilon_i = \frac{f_A\tau_A}{(E_\omega - E_A)^2 + \tau_A^2} + \frac{f_B\tau_B}{(E_\omega - E_B)^2 + \tau_B^2} + \frac{f_b}{E_\omega}\Theta(E_\omega - E_g, \tau_b)$$

where τ_A (28 meV) and τ_B (42 meV) are the bandwidth of exciton A and exciton B. E_A (1.884 eV) and E_B (2.02 eV) are the transition energy of exciton A and exciton B. f_A (0.32 meV) and f_B (0.43 meV) are the equivalent oscillator strength of exciton A (B). τ_b (0.398 eV), E_g (2.43 eV), and f_b (59) are the line width, band gap, and equivalent oscillator strength of the interband transition, respectively.

$$\Theta(x, \tau) = \int_{-\infty}^{x} \frac{\tau}{\tau^2 + \theta^2} \mathrm{d}\theta$$

is a step function with a stretched bandwidth τ.

$$\epsilon_r(\omega) = \epsilon_r + \frac{1}{\pi}\int_0^\infty \frac{s\epsilon_i}{s^2 - \omega^2} \mathrm{d}s$$

where ϵ_r is the static dielectric constant. The real part of the refraction then can be calculated using the Kramers–Kronig relation.

Conflict of Interest: The authors declare no competing financial interest.

Acknowledgment. This work was supported by National Science Foundation of China (Grant Nos. 61422501 and 11374023), the National Basic Research Program of China (973 Program, Grant No. 2015CB932403), the Beijing Natural Science Foundation (Grant No. L140007), the Robert A. Welch Foundation under Grant C-1222, and by the U.S. Army Research Office MURI Grant W911NF-11-1-0362.

Supporting Information Available: The Supporting Information is available free of charge on the ACS Publications website at DOI: 10.1021/acsnano.5b03764.

Additional figures and experimental details (PDF)

REFERENCES AND NOTES

1. Najmaei, S.; Liu, Z.; Zhou, W.; Zou, X.; Shi, G.; Lei, S.; Yakobson, B. I.; Idrobo, J. C.; Ajayan, P. M.; Lou, J. Vapour Phase Growth and Grain Boundary Structure of Molybdenum Disulphide Atomic Layers. *Nat. Mater.* **2013**, *12*, 754–759.
2. Wang, Q. H.; Kalantar-Zadeh, K.; Kis, A.; Coleman, J. N.; Strano, M. S. Electronics and Optoelectronics of Two-Dimensional Transition Metal Dichalcogenides. *Nat. Nanotechnol.* **2012**, *7*, 699–712.
3. Mak, K. F.; He, K.; Lee, C.; Lee, G. H.; Hone, J.; Heinz, T. F.; Shan, J. Tightly Bound Trions in Monolayer MoS_2. *Nat. Mater.* **2013**, *12*, 207–211.
4. Eda, G.; Yamaguchi, H.; Voiry, D.; Fujita, T.; Chen, M.; Chhowalla, M. Photoluminescence from Chemically Exfoliated MoS_2. *Nano Lett.* **2011**, *11*, 5111–5116.
5. Splendiani, A.; Sun, L.; Zhang, Y.; Li, T.; Kim, J.; Chim, C. Y.; Galli, G.; Wang, F. Emerging Photoluminescence in Monolayer MoS_2. *Nano Lett.* **2010**, *10*, 1271–1275.
6. Newaz, A. K. M.; Prasai, D.; Ziegler, J. I.; Caudel, D.; Robinson, S.; Haglund, R. F., Jr.; Bolotin, K. I. Electrical Control of Optical Properties of Monolayer MoS_2. *Solid State Commun.* **2013**, *155*, 49–52.
7. Lin, J. D.; Han, C.; Wang, F.; Wang, R.; Xiang, D.; Qin, S.; Zhang, X. A.; Wang, L.; Zhang, H.; Wee, A. T. S.; et al. Electron-Doping-Enhanced Trion Formation in Monolayer Molybdenum Disulfide Functionalized with Cesium Carbonate. *ACS Nano* **2014**, *8*, 5323–5329.
8. Ross, J. S.; Wu, S.; Yu, H.; Ghimire, N. J.; Jones, A. M.; Aivazian, G.; Yan, J.; Mandrus, D. G.; Xiao, D.; Yao, W.; et al. Electrical Control of Neutral and Charged Excitons in a Monolayer Semiconductor. *Nat. Commun.* **2013**, *4*, 1474.
9. Tongay, S.; Zhou, J.; Ataca, C.; Liu, J.; Kang, J. S.; Matthews, T. S.; You, L.; Li, J.; Grossman, J. C.; Wu, J. Broad-range Modulation of Light Emission in Two-Dimensional Semiconductors by Molecular Physisorption Gating. *Nano Lett.* **2013**, *13*, 2831–2836.
10. Sreeprasad, T. S.; Nguyen, P.; Kim, N.; Berry, V. Controlled, Defect-Guided, Metal-Nanoparticle Incorporation onto MoS_2 *via* Chemical and Microwave Routes: Electrical, Thermal, and Structural Properties. *Nano Lett.* **2013**, *13*, 4434–4441.
11. Mouri, S.; Miyauchi, Y.; Matsuda, K. Tunable Photoluminescence of Monolayer MoS_2 *via* Chemical Doping. *Nano Lett.* **2013**, *13*, 5944–5948.
12. Liu, J. T.; Wang, T. B.; Li, X. J.; Liu, N. H. Enhanced Absorption of Monolayer MoS_2 with Resonant Back Reflector. *J. Appl. Phys.* **2014**, *115*, 193511.
13. Liu, X.; Galfsky, T.; Sun, Z.; Xia, F.; Lin, E. C.; Lee, Y. H.; Kéna-Cohen, S.; Menon, V. M. Strong Light-Matter Coupling in Two-Dimensional Atomic Crystals. *Nat. Photonics* **2014**, *9*, 30–34.
14. Wu, S.; Buckley, S.; Schaibley, J. R.; Feng, L.; Yan, J.; Mandrus, D. G.; Hatami, F.; Yao, W.; Vučković, J.; Majumdar, A.; et al. Monolayer Semiconductor Nanocavity Lasers with Ultralow Thresholds. *Nature* **2015**, *520*, 69–72.
15. Righini, M.; Volpe, G.; Girard, C.; Petrov, D.; Quidant, R. Surface Plasmon Optical Tweezers: Tunable Optical Manipulation in the Femtonewton Range. *Phys. Rev. Lett.* **2008**, *100*, 186804.
16. Juan, M. L.; Righini, M.; Quidant, R. Plasmon Nano-optical Tweezers. *Nat. Photonics* **2011**, *5*, 349–356.
17. Munday, J. N.; Atwater, H. A. Large Integrated Absorption Enhancement in Plasmonic Solar Cells by Combining Metallic Gratings and Antireflection Coatings. *Nano Lett.* **2011**, *11*, 2195–2201.
18. Alemu, N.; Chen, F. Plasmon-Enhanced Light Absorption of Thin-Film Solar Cells Using Hemispherical Nanoparticles. *Phys. Status Solidi A* **2014**, *211*, 213–218.
19. Chen, P. Y.; Alù, A. Atomically-Thin Surface Cloak Using Graphene Monolayers. *ACS Nano* **2011**, *5*, 5855–5863.
20. Emani, N. K.; Chung, T.; Kildishev, A. V.; Shalaev, V. M.; Chen, Y. P.; Boltasseva, A. Electrical Modulation of Fano Resonance in Plasmonic Nanostructures Using Graphene. *Nano Lett.* **2014**, *14*, 78–82.

21. Zhu, X.; Shi, L.; Schmidt, M. S.; Boisen, A.; Hansen, O.; Zi, J.; Xiao, S.; Mortensen, N. A. Enhanced Light-Matter Interactions in Graphene-Covered Gold Nanovoid Arrays. *Nano Lett.* **2013**, *13*, 4690–4696.
22. Brongersma, M. L.; Halas, N. J.; Nordlander, P. Plasmon-Induced Hot Carrier Science and Technology. *Nat. Nanotechnol.* **2015**, *10*, 25–34.
23. Kale, M. J.; Avanesian, T.; Christopher, P. Direct Photocatalysis by Plasmonic Nanostructures. *ACS Catal.* **2014**, *4*, 116–128.
24. Fang, Z.; Liu, Z.; Wang, Y.; Ajayan, P. M.; Nordlander, P.; Halas, N. J. Graphene-Antenna Sandwich Photodetector. *Nano Lett.* **2012**, *12*, 3808–3813.
25. Kang, Y.; Najmaei, S.; Liu, Z.; Bao, Y.; Wang, Y.; Zhu, X.; Halas, N. J.; Nordlander, P.; Ajayan, P. M.; Lou, J.; et al. Plasmonic Hot Electron Induced Structural Phase Transition in a MoS_2 Monolayer. *Adv. Mater.* **2014**, *26*, 6467–6471.
26. Sun, Y.; Liu, K.; Hong, X.; Chen, M.; Kim, J.; Shi, S.; Wu, J.; Zettl, A.; Wang, F. Probing Local Strain at MX_2-Metal Boundaries with Surface Plasmon-Enhanced Raman Scattering. *Nano Lett.* **2014**, *14*, 5329–5334.
27. Wang, Y.; Ou, J. Z.; Chrimes, A. F.; Carey, B. J.; Daeneke, T.; Alsaif, M. M.; Mortazavi, M.; Zhuiykov, S.; Medhekar, N.; Bhaskaran, M.; et al. Plasmon Resonances of Highly Doped Two-Dimensional MoS_2. *Nano Lett.* **2015**, *15*, 883–890.
28. Mitioglu, A. A.; Plochocka, P.; Jadczak, J. N.; Escoffier, W.; Rikken, G. L. J. A.; Kulyuk, L.; Maude, D. K. Optical Manipulation of the Exciton Charge State in Single-Layer Tungsten Disulfide. *Phys. Rev. B: Condens. Matter Mater. Phys.* **2013**, *88*, 245403.
29. Dhakal, K. P.; Duong, D. L.; Lee, J.; Nam, H.; Kim, M.; Kan, M.; Lee, Y. H.; Kim, J. Confocal Absorption Spectral Imaging of MoS_2: Optical Transitions Depending on the Atomic Thickness of Intrinsic and Chemically Doped MoS_2. *Nanoscale* **2014**, *6*, 13028–13035.
30. Lin, Y.; Ling, X.; Yu, L.; Huang, S.; Hsu, A. L.; Lee, Y. H.; Kong, J.; Dresselhaus, M. S.; Palacios, T. Dielectric Screening of Excitons and Trions in Single-Layer MoS_2. *Nano Lett.* **2014**, *14*, 5569–5576.
31. He, K.; Kumar, N.; Zhao, L.; Wang, Z.; Mak, K. F.; Zhao, H.; Shan, J. Tightly Bound Excitons in Monolayer WSe_2. *Phys. Rev. Lett.* **2014**, *113*, 026803.
32. Ramasubramaniam, A. Large Excitonic Effects in Monolayers of Molybdenum and Tungsten Dichalcogenides. *Phys. Rev. B: Condens. Matter Mater. Phys.* **2012**, *86*, 115409.
33. Feng, J.; Qian, X.; Huang, C.; Li, J. Strain-Engineered Artificial Atom as a Broad-Spectrum Solar Energy Funnel. *Nat. Photonics* **2012**, *6*, 866–872.
34. Klots, A. R.; Newaz, A. K. M.; Wang, B.; Prasai, D.; Krzyzanowska, H.; Lin, J.; Caudel, D.; Ghimire, N. J.; Yan, J.; Ivanov, B. L.; et al. Probing excitonic states in suspended two-dimensional semiconductors by photocurrent spectroscopy. *Sci. Rep.* **2014**, *4*, 6608.
35. Najmaei, S.; Liu, Z.; Zhou, W.; Zou, X.; Shi, G.; Lei, S.; Yakobson, B. I.; Idrobo, J. C.; Ajayan, P. M.; Lou, J. Vapour Phase Growth and Grain Boundary Structure of Molybdenum Disulphide Atomic Layers. *Nat. Mater.* **2013**, *12*, 754–759.